

MOLECULAR POLYMORPHISM: MICROWAVE SPECTRA,
EQUILIBRIUM STRUCTURES, AND AN ASTRONOMICAL
INVESTIGATION OF THE HNCS ISOMERIC FAMILY.

SUPPLEMENTARY MATERIAL

Brett A. McGuire, Marie-Aline Martin-Drumel, Sven Thorwirth, Sandra Brünken, Valerio Lattanzi, Justin L. Neill, Silvia Spezzano, Zhenhong Yu, Daniel P. Zaleski, Anthony J. Remijan, Brooks H. Pate, and Michael C. McCarthy

Table of Contents

Pg. 3 Molecular Identifications in the CP-FTMW Spectrum

Pg. 4 Measured Rotational Transitions

Pg. 15 Molecular Structures

Pg. 17 Derived Semi-experimental Rotational Constants

Pg. 22 Astrophysical Analysis

LIST OF TABLES

S1	Molecules identified in the high-band chirped-pulse spectrum.	3
S2	Measured Rotational Transitions of HSCN, H ³⁴ SCN, HS ¹³ CN, and DSC ¹⁵ N (in MHz).	4
S3	Rotational Transitions of DSCN and D ³⁴ SCN (in MHz).	6
S4	Measured Rotational Transitions of HCNS and HCN ³⁴ S (in MHz).	10
S5	Measured Rotational Transitions of H ¹³ CNS (in MHz).	11
S6	Measured Rotational Transitions of DCNS (in MHz).	12
S7	Measured Rotational Transitions of HSNC, H ³⁴ SNC, and HSN ¹³ C (in MHz). .	13
S8	Measured Rotational Transitions of DSNC (in MHz).	14
S9	Rotational Transitions of HSC ¹⁵ N, HC ¹⁵ NS, and HS ¹⁵ NC (in MHz).	14
S10	Experimental and Calculated Structures for HSCN.	15
S11	Experimental and Calculated Structures for HCNS.	15
S12	Experimental and Calculated Structures for HNCS.	16
S13	Experimental and Calculated Structures for HSNC.	16
S14	Vibrational corrections, semi-experimental rotational constants and corre- sponding inertial defects of isotopic HNCS (in MHz).	18
S15	Vibrational corrections, semi-experimental rotational constants and corre- sponding inertial defects of isotopic HSCN (in MHz).	19
S16	Vibrational corrections and semi-experimental rotational constants of isotopic HCNS (in MHz).	20
S17	Vibrational corrections and semi-experimental rotational constants of isotopic HSNC (in MHz).	21

LIST OF FIGURES

S1	Measurements of the continuum temperature (T_c) in Sgr B2(N) at various frequencies from Hollis et al. (2007), Belloche et al. (2013), and Neill et al. (2014).	24
S2	Qualitative schematic of HSCN in Sgr B2(N).	25

MOLECULAR IDENTIFICATIONS IN CHIRPED PULSE SPECTRA

TABLE S1. Molecules identified in the high-band chirped-pulse spectrum.

Number of Atoms	Molecule	Interstellar
2	SH	Y
3	SSH	N
	NCS	N
	SO ₂	Y
	OCS	Y
4	HSCN	Y
	HNCS	N
	H ₂ CS	Y
	CCCS	Y
5	HCCCN	Y
	HCCNC	Y
	CH ₂ CN	Y
	H ₂ CCS	N
	HCSCN	N
6	CH ₃ NC	Y
	CH ₃ SH	Y
	H ₂ CCNH	Y
7	CH ₂ CHCN	Y
	CH ₂ CHNC	N
	HSCH ₂ CN	N
	CH ₃ CCH	Y
8	CH ₃ CCCN	Y
	H ₂ CCCHCN	Y
9	CH ₃ CH ₂ CN	Y

MEASURED ROTATIONAL TRANSITIONS

TABLE S2: Measured Rotational Transitions of HSCN,
 H^{34}SCN , HS^{13}CN , and DSC^{15}N (in MHz).

Transition		Frequency ¹			
$J'_{K'_a,K'_c} \rightarrow J''_{K''_a,K''_c}$	$F' \rightarrow F''$	HSCN ²	H^{34}SCN	HS^{13}CN	DSC^{15}N
$1_{0,1} \rightarrow 0_{0,0}$	$1 \rightarrow 1$	11468.633	11213.181	11410.458	10791.195
	$2 \rightarrow 1$	11469.851	11214.398	11411.674	10791.209
	$0 \rightarrow 1$	11471.669	11216.218	11413.495	10791.235
$2_{1,2} \rightarrow 1_{1,1}$	$2 \rightarrow 1$	22817.864	22312.014	22702.715	21381.218
	$1 \rightarrow 1$	22818.474		22703.327	21381.181
	$2 \rightarrow 2$	22818.711		22703.563	21381.259
	$3 \rightarrow 2$	22819.107	22313.256	22703.956	21381.239
	$1 \rightarrow 0$	22820.591	22314.741	22705.443	21381.282
$2_{0,2} \rightarrow 1_{0,1}$	$2 \rightarrow 2$	22937.998	22427.100	22821.650	21582.154
	$1 \rightarrow 0$	22938.201	22427.302	22821.855	21582.154
	$2 \rightarrow 1$	22939.214	22428.322	22822.867	21582.175
	$3 \rightarrow 2$	22939.302	22428.408	22822.957	
$2_{1,1} \rightarrow 1_{1,0}$	$2 \rightarrow 1$	23057.406	22541.513		21782.446
	$2 \rightarrow 2$	23057.769			
	$3 \rightarrow 2$	23058.682	22542.786		21782.469
	$1 \rightarrow 1$	23058.819			21782.516
	$1 \rightarrow 0$	23059.735	22543.840		21782.450
$3_{1,3} \rightarrow 2_{1,2}$	$3 \rightarrow 3$	34227.537	33468.772		
	$3 \rightarrow 2$	34227.938	33469.170	34055.217	32071.642
	$4 \rightarrow 3$	34228.291	33469.522	34055.570	32071.642
	$2 \rightarrow 1$	34228.326	33469.561		32071.642
	$2 \rightarrow 2$	34228.936			
$3_{0,3} \rightarrow 2_{0,2}$	$3 \rightarrow 3$	34407.326	33640.990	34232.804	
	$2 \rightarrow 1$	34408.424	33642.086	34233.915	32372.657

Continued on next page

TABLE S2 – continued from previous page

Transition ¹		HSCN ²	H ³⁴ SCN	HS ¹³ CN	DSC ¹⁵ N
$J'_{K'_a, K'_c} \rightarrow J''_{K''_a, K''_c}$	$F' \rightarrow F''$				
	3 → 2	34408.629	33642.291	34234.109	32372.657
	4 → 3	34408.678	33642.342	34234.160	32372.657
	2 → 2	34410.447	33644.109	34235.929	
$3_{1,2} \rightarrow 2_{1,1}$	3 → 3	34586.340			
	3 → 2	34587.252	33813.418	34410.969	32673.478
	2 → 1	34587.564	33813.729	34411.275	32673.478
	4 → 3	34587.625	33813.787	34411.342	32673.478
	2 → 2	34588.978	33815.139		

¹ Estimated (1σ) measurement uncertainties are 2 kHz (for microwave transitions) and 70 kHz (for mm-wave transitions).

² From Brünken et al. 2009.

TABLE S3: Rotational Transitions of DSCN and D³⁴SCN
(in MHz).

Transition			Frequency ¹	
$J'_{K'_a, K'_c} \rightarrow J''_{K''_a, K''_c}$	$F'_1 \rightarrow F''_1$	$F' \rightarrow F''$	DSCN ²	D ³⁴ SCN
$1_{0,1} \rightarrow 0_{0,0}$	$1 \rightarrow 1$	$0 \rightarrow 1$		10958.858
		$2 \rightarrow 1$	11193.327	10958.874
		$0 \rightarrow 1$	11193.327	10958.874
		$1 \rightarrow 0$	11193.338	10958.884
		$1 \rightarrow 1$	11193.338	10958.884
		$1 \rightarrow 2$	11193.338	10958.884
	$2 \rightarrow 1$	$2 \rightarrow 1$	11194.538	10960.084
		$2 \rightarrow 2$	11194.538	10960.084
		$3 \rightarrow 2$	11194.549	10960.098
		$1 \rightarrow 0$	11194.562	10960.106
		$1 \rightarrow 1$	11194.562	10960.106
	$0 \rightarrow 1$	$1 \rightarrow 2$	11196.371	10961.916
		$1 \rightarrow 0$	11196.371	10961.916
		$1 \rightarrow 1$	11196.371	10961.916
$2_{1,2} \rightarrow 1_{1,1}$	$2 \rightarrow 1$	$1 \rightarrow 0$	22171.174	21710.416
		$3 \rightarrow 2$	22171.213	21710.449
		$2 \rightarrow 1$	22171.243	21710.480
	$1 \rightarrow 1$	$2 \rightarrow 2$	22171.822	21711.060
	$2 \rightarrow 2$	$3 \rightarrow 3$	22172.069	
	$3 \rightarrow 2$	$3 \rightarrow 2$	22172.452	21711.688
		$4 \rightarrow 3$	22172.464	21711.697
		$2 \rightarrow 1$	22172.478	21711.707
	$1 \rightarrow 0$	$2 \rightarrow 1$	22173.951	21713.186
		$1 \rightarrow 1$	22173.962	
$2_{0,2} \rightarrow 1_{0,1}$	$2 \rightarrow 2$	$2 \rightarrow 2$	22387.189	21918.304

Continued on next page

TABLE S3 – continued from previous page

Transition		Frequency ¹	
$J'_{K'_a,K'_c} \rightarrow J''_{K''_a,K''_c}$		$F'_1 \rightarrow F''_1$	DSCN ²
		3 → 3	22387.189
		1 → 1	22387.189
1 → 0	1 → 1	22387.385	21918.499
	2 → 1	22387.396	21918.510
	0 → 1		21918.526
2 → 1	2 → 1		21919.506
	3 → 2	22388.413	21919.526
3 → 2	4 → 3	22388.496	21919.611
	2 → 1	22388.496	
	3 → 2	22388.496	
1 → 1	1 → 1	22390.413	21921.529
	2 → 1	22390.424	21921.540
	1 → 2	22390.424	21921.540
	2 → 2	22390.438	21921.550
	1 → 0	22390.438	21921.553
	0 → 1	22390.438	21921.553
$2_{1,1} \rightarrow 1_{1,0}$	2 → 1	22602.890	22125.891
	3 → 2	22602.926	22125.924
	1 → 0	22602.955	22125.950
2 → 2	2 → 1	22603.253	
	3 → 3	22603.285	22126.281
	2 → 2		22126.281
3 → 2	3 → 2	22604.174	22127.173
	4 → 3	22604.205	22127.204
	2 → 1	22604.205	22127.204
1 → 0	1 → 1	22605.233	22128.231

Continued on next page

TABLE S3 – continued from previous page

Transition		Frequency ¹		
$J'_{K'_a, K'_c} \rightarrow J''_{K''_a, K''_c}$		$F'_1 \rightarrow F''_1$	$F' \rightarrow F''$	DSCN ²
		2 → 1	22605.255	22128.256
		0 → 1	22605.286	
$3_{1,3} \rightarrow 2_{1,2}$	$3 \rightarrow 3$	4 → 4	33257.463	
		4 → 3	33257.854	32566.727
		3 → 2	33257.854	32566.727
		2 → 1	33257.854	32566.727
	4 → 3	5 → 4	33258.207	32567.082
		3 → 2	33258.207	32567.082
		4 → 3		32567.082
	2 → 1	3 → 2	33258.244	
		2 → 1	33258.244	
$3_{0,3} \rightarrow 2_{0,2}$	$3 \rightarrow 3$	2 → 2	33580.615	32877.330
		4 → 4	33580.615	32877.330
		3 → 3	33580.615	32877.330
	2 → 1	3 → 2		32878.432
	3 → 2	2 → 1	33581.922	32878.637
		4 → 3	33581.922	32878.637
	4 → 3	3 → 2	33581.969	32878.685
		5 → 4	33581.969	32878.685
		4 → 3	33581.969	32878.685
	2 → 2	3 → 3		32880.455
$3_{1,2} \rightarrow 2_{1,1}$	$3 \rightarrow 3$	3 → 3	33904.487	
		2 → 2	33904.487	
		4 → 4	33904.487	
	3 → 2	3 → 2	33905.387	
		4 → 3	33905.408	33189.920

Continued on next page

TABLE S3 – continued from previous page

Transition	Frequency ¹		
$J'_{K'_a, K'_c} \rightarrow J''_{K''_a, K''_c}$	$F'_1 \rightarrow F''_1$	$F' \rightarrow F''$	DSCN ²
	2 → 1	33905.408	33189.920
	2 → 1	2 → 1	33905.697
		3 → 2	33905.719
	4 → 3	4 → 3	33905.767
		5 → 4	33905.775
		3 → 2	33190.289
	2 → 2	3 → 3	33907.131

¹ The coupling scheme $F_1 = J + I(\text{N})$, $F = F_1 + I(\text{D})$ was used. Estimated (1σ) measurement uncertainties are 2 kHz.

² From Brünken et al. 2009.

TABLE S4. Measured Rotational Transitions of HCNS and HCN³⁴S (in MHz).

Transition		Frequency ^a	
$J' \rightarrow J''$	$F' \rightarrow F''$	HCNS	HCN ³⁴ S
1 → 0	1 → 1	12302.699	12017.576
	2 → 1	12302.918	12017.794
	0 → 1	12303.241	12018.117
2 → 1	2 → 2	24605.501	
	1 → 0	24605.539	
	2 → 1	24605.719	
	3 → 2	24605.738	
3 → 2	1 → 1	24606.081	
	3 → 3	36908.243	
	2 → 1	36908.442	
	3 → 2	36908.477	
	4 → 3	36908.490	
	2 → 2	36908.800	

^a Estimated (1σ) measurement uncertainties are 2 kHz.

TABLE S5. Measured Rotational Transitions of H¹³CNS (in MHz).

$J' \rightarrow J''$	Transition		Frequency ^a
	$F'_1 \rightarrow F''_1$	$F' \rightarrow F''$	
1 → 0	1 → 1	1/2 → 1/2	11862.563
		1/2 → 3/2	11862.563
		3/2 → 1/2	11862.573
		3/2 → 3/2	11862.573
	2 → 1	3/2 → 1/2	11862.784
		3/2 → 3/2	11862.784
		5/2 → 3/2	11862.798
	0 → 1	1/2 → 1/2	11863.117
		1/2 → 3/2	11863.117
2 → 1	2 → 2	3/2 → 3/2	23725.257
		5/2 → 5/2	23725.257
	1 → 0	3/2 → 1/2	23725.296
	2 → 1	5/2 → 3/2	23725.477
	3 → 2	5/2 → 3/2	23725.477
		7/2 → 5/2	23725.495
		3/2 → 3/2	23725.841
	4 → 3	7/2 → 5/2	35588.123
		9/2 → 7/2	35588.123
		7/2 → 5/2	35588.123

^a The coupling scheme $F_1 = J + I(\text{N})$, $F = F_1 + I(^{13}\text{C})$ was used. Estimated (1σ) measurement uncertainties are 2 kHz.

TABLE S6. Measured Rotational Transitions of DCNS (in MHz).

$J' \rightarrow J''$	Transition		Frequency ^a
	$F'_1 \rightarrow F''_1$	$F' \rightarrow F''$	
$1 \rightarrow 0$	$1 \rightarrow 1$	$0 \rightarrow 1$	11235.534
		$1 \rightarrow 1$	11235.534
		$2 \rightarrow 1$	11235.534
		$1 \rightarrow 2$	11235.574
		$2 \rightarrow 2$	11235.574
	$2 \rightarrow 1$	$0 \rightarrow 1$	11235.767
		$1 \rightarrow 1$	11235.767
		$2 \rightarrow 3$	11235.783
		$1 \rightarrow 2$	11235.828
		$2 \rightarrow 2$	11235.828
	$0 \rightarrow 1$	$0 \rightarrow 1$	11236.121
		$1 \rightarrow 1$	11236.121
		$2 \rightarrow 1$	11236.121
$2 \rightarrow 1$	$2 \rightarrow 2$	$2 \rightarrow 2$	22471.239
	$1 \rightarrow 0$	$1 \rightarrow 0$	22471.239
	$2 \rightarrow 1$	$2 \rightarrow 3$	22471.466
	$3 \rightarrow 2$	$1 \rightarrow 2$	22471.487
		$3 \rightarrow 4$	22471.487
		$2 \rightarrow 3$	22471.503
	$2 \rightarrow 1$	$1 \rightarrow 2$	22471.532
$3 \rightarrow 2$	$2 \rightarrow 1$	$2 \rightarrow 3$	33707.088
		$0 \rightarrow 1$	33707.114
		$1 \rightarrow 2$	33707.114
	$3 \rightarrow 2$	$1 \rightarrow 2$	33707.124
		$3 \rightarrow 4$	33707.124
	$4 \rightarrow 3$	$4 \rightarrow 5$	33707.139
		$2 \rightarrow 3$	33707.139
		$3 \rightarrow 4$	33707.139
	$3 \rightarrow 2$	$2 \rightarrow 3$	33707.146

^a The coupling scheme $F_1 = J + I(\text{N})$, $F = F_1 + I(\text{D})$ was used. Estimated (1σ) measurement

uncertainties are 2 kHz.

TABLE S7. Measured Rotational Transitions of HSNC, H³⁴SNC, and HSN¹³C (in MHz).

Transition		Frequency ^a		
$J'_{K'_a,K'_c} \rightarrow J''_{K''_a,K''_c}$	$F' \rightarrow F$	HSNC	H ³⁴ SNC	HSN ¹³ C
$1_{0,1} \rightarrow 0_{0,0}$	$0 \rightarrow 1$	12557.441	12282.670	12044.132
	$2 \rightarrow 1$	12557.989	12283.220	12044.682
	$1 \rightarrow 1$	12558.353	12283.583	12045.045
$2_{0,2} \rightarrow 1_{0,1}$	$1 \rightarrow 1$	25115.382		
	$3 \rightarrow 2$	25115.965		24089.367
	$2 \rightarrow 1$	25115.991		24089.394
	$1 \rightarrow 0$	25116.293		24089.691
	$2 \rightarrow 2$	25116.352		24089.752
$3_{0,3} \rightarrow 2_{0,2}$	$2 \rightarrow 2$	37673.168		
	$4 \rightarrow 3$	37673.700		36133.831
	$3 \rightarrow 2$	37673.717		36133.850
	$2 \rightarrow 1$	37673.777		36133.907
	$3 \rightarrow 3$	37674.102		

^a Estimated (1σ) measurement uncertainties are 2 kHz.

TABLE S8. Measured Rotational Transitions of DSNC (in MHz).

$J'_{K'_a,K'_c} \rightarrow J''_{K''_a,K''_c}$	Transition		Frequency ^a
	$F'_1 \rightarrow F''_1$	$F' \rightarrow F$	
$1_{0,1} \rightarrow 0_{0,0}$	$0 \rightarrow 1$	$1 \rightarrow 0$	12235.580
		$1 \rightarrow 1$	12235.580
		$1 \rightarrow 2$	12235.580
	$2 \rightarrow 1$	$2 \rightarrow 2$	12236.115
		$2 \rightarrow 1$	12236.115
		$3 \rightarrow 2$	12236.126
		$1 \rightarrow 0$	12236.134
		$1 \rightarrow 1$	12236.134
	$1 \rightarrow 1$	$2 \rightarrow 1$	12236.482
		$2 \rightarrow 2$	12236.482
		$1 \rightarrow 0$	12236.491
		$1 \rightarrow 1$	12236.491
		$1 \rightarrow 2$	12236.491
$2_{0,2} \rightarrow 1_{0,1}$	$3 \rightarrow 2$	$3 \rightarrow 2$	24471.955
		$2 \rightarrow 1$	24471.955
		$4 \rightarrow 3$	24471.955
$3_{0,3} \rightarrow 2_{0,2}$	$4 \rightarrow 3$	$4 \rightarrow 3$	36706.988
		$3 \rightarrow 2$	36706.988
		$5 \rightarrow 4$	36706.988

^a The coupling scheme $F_1 = J + I(\text{N})$, $F = F_1 + I(\text{D})$ was used. Estimated (1σ) measurement uncertainties are 2 kHz.

 TABLE S9. Rotational Transitions of HSC¹⁵N, HC¹⁵NS, and HS¹⁵NC (in MHz).

Transition ^a	HSC ¹⁵ N	HC ¹⁵ NS	HS ¹⁵ NC
$1 \rightarrow 0$	11055.708	12251.421	12485.022
$2 \rightarrow 1$	22111.347		24969.938
$3 \rightarrow 2$	33166.844		

^a For HSC¹⁵N and HS¹⁵NC, the transition is $J'_{0,J'} \rightarrow J''_{0,J''}$ and simply $J' \rightarrow J$ for HC¹⁵NS. Estimated (1σ) measurement uncertainties are 2 kHz.

MOLECULAR STRUCTURES

TABLE S10. Experimental and Calculated Structures for HSCN.

Parameter ^a	r_0	r_e^{SE}	r_e
$r(\text{HS})$	1.342(9)	1.340(1)	
$r(\text{SC})$	1.708(13)	1.699(3)	
$r(\text{CN})$	1.152(19)	1.153(4)	
$\theta(\text{HSC})$	92.8(7)	94.3(4)	
$\theta(\text{SCN})$	171.0(25)	175.8(12)	

^a Planar geometry assumed, and the dihedral angle $\phi(\text{HSCN})$ was constrained to 180°. Bond lengths are in Å, angles are in degrees (°). Formal, statistical uncertainties (in parentheses) are 1σ in units of the last significant digit.

TABLE S11. Experimental and Calculated Structures for HCNS.

Parameter ^a	r_0	r_e^{SE}	r_e
$r(\text{HC})$	1.051(1)	1.059(1)	
$r(\text{CN})$	1.169(3)	1.160(2)	
$r(\text{NS})$	1.593(3)	1.600(2)	

^a Bond lengths are in Å. Formal, statistical uncertainties (in parentheses) are 1σ in units of the last significant digit.

TABLE S12. Experimental and Calculated Structures for HNCS.

Parameter ^a	$r_s^{m,b}$	r_0	r_e^{SE}	r_e
$r(\text{HN})$	0.993(6)	0.961(7)	0.993(13)	
$r(\text{NC})$	1.207(2)	1.215(10)	1.205(17)	
$r(\text{CS})$	1.566(1)	1.563(8)	1.568(13)	
$\theta(\text{HNC})$	131.7(19)	130.5(53)	131.0(8)	
$\theta(\text{NCS})$	173.8(23)	173(15)	172.7(26)	

^a Planar geometry assumed, and the dihedral angle $\phi(\text{HSCN})$ was constrained to 180°. Bond lengths are in Å, angles are in degrees (°). Formal, statistical uncertainties (in parentheses) are 1σ in units of the last significant digit.

^b Ref [31].

TABLE S13. Experimental and Calculated Structures for HSNC.

Parameter ^a	r_0	r_e^{SE}	r_e
$r(\text{HS})$	1.327(2)	1.324(3)	
$r(\text{SN})$	1.660(1)	1.661(2)	
$r(\text{NC})$	1.175(2)	1.171(3)	
$\theta(\text{HSN})$	95.37 ^b	95.37 ^b	95.37
$\theta(\text{SNC})$	173.7 ^b	173.7 ^b	173.7

^a Planar geometry assumed, and the dihedral angle $\phi(\text{HSCN})$ was constrained to 180°. Bond lengths are in Å, angles are in degrees (°). Formal, statistical uncertainties (in parentheses) are 1σ in units of the last significant digit.

^c Fixed to theoretical value.

ROTATIONAL CONSTANTS

TABLE S14. Vibrational corrections, semi-experimental rotational constants and corresponding inertial defects of isotopic HNCS (in MHz).

Constant ^a	HNCS	H ¹⁵ NCS	HN ¹³ CS	HN ³⁴ S	DNCS
A_0	1357250	1339170	1352250	1357100	705510.74
B_0	5883.463	5688.695	5864.552	5744.833	5500.439
C_0	5845.611	5652.983	5826.888	5708.736	5445.225
fc-CCSD(T)/cc-PV(T+d)Z vibrational corrections:					
ΔA	-133661.104	-131798.280	-133405.113	-133600.866	-58918.982
ΔB	19.298	18.403	19.035	18.762	17.225
ΔC	22.645	21.541	22.354	21.958	21.080
A_e^{emp}	1223588.896	1207371.720	1220844.887	1223499.134	646591.758
B_e^{emp}	5902.760	5707.099	5883.588	5763.594	5517.664
C_e^{emp}	5868.257	5674.524	5849.242	5730.694	5466.306

^a Experimental rotational constants from Ref [31].

TABLE S15. Vibrational corrections, semi-experimental rotational constants and corresponding inertial defects of isotopic HSCN (in MHz).

Constant ^a	HSCN ^b	H ³⁴ SCN	HS ¹³ CN	HSC ¹⁵ N	DSCN	D ³⁴ SCN	DSC ¹⁵ N
A_0	289630	289500 ^b	289500 ^b	289500 ^c	150997	148872	150535
B_0	5794.714	5664.476	5765.030	5705.099	5585.586	5583.813	5495.912
C_0	5674.939	5549.726	5646.447	5470.134	5489.250	5376.083	5295.300
Δ_0^c	0.0958	0.0990	0.0953	0.1639	0.1364	0.1025	0.1265
fc-CCSD(T)/cc-PV(T+d)Z vibrational corrections:							
ΔA	1663.332	1657.975	1668.604	1663.038	556.041	556.114	556.933
ΔB	8.501	8.224	8.542	8.077	6.985	6.757	6.654
ΔC	14.632	14.094	14.605	13.794	14.758	14.233	13.912
A_e^{emp}	291292.332	291157.975	291168.604	291163.038	151553.041	149428.114	151091.933
B_e^{emp}	5803.215	5672.700	5773.573	5593.663	5712.084	5590.570	5502.566
C_e^{emp}	5689.571	5563.820	5661.052	5483.928	5504.008	5390.316	5309.212
$\Delta_e^{emp\; c}$	0.0045	0.0077	0.0041	0.0722	0.0101	-0.0237	0.0000

^a Experimental rotational constants from Table 1 in the main text.^b Fixed to value derived for normal HSCN.^c Inertial defect in units of amu Å².

TABLE S16. Vibrational corrections and semi-experimental rotational constants of isotopic HCNS (in MHz).

Constant ^a	HCNS	H ¹³ CNS	HC ¹⁵ NS	HCN ³⁴ S	DCNS
B_0	6151.4436(4)	5931.3801(4)	6125.714(1)	6008.8818(6)	5617.8801(3)
fc-CCSD(T)/cc-PV(T+d)Z vibrational corrections:					
ΔB	-2.951	-1.863	-3.330	-3.181	-4.057
B_e^{emp}	6148.493	5929.517	6122.384	6005.701	5613.823

^a Experimental rotational constants from Table 2 in the main text.^b $B_e^{emp} = B_0 + \Delta B$

TABLE S17. Vibrational corrections and semi-experimental rotational constants of isotopic HSNC (in MHz).

Constant ^a	HSNC	H ³⁴ SNC	HS ³⁵ NC	HSN ¹³ C	DSNC
(B_0) _{eff}	6279.0335(4)	6141.6485(6)	6242.520(1)	6022.3790(3)	6118.1242(4)
($B_0 + C_0$) _{eff}	12558.067	12283.297	12485.04	12044.758	12236.2484
fc-CCSD(T)/cc-PV(T+d)Z vibrational corrections:					
ΔB	8.85	8.85	8.85	8.85	8.85
ΔC	16.187	16.187	16.187	16.187	16.187
$\Delta(B + C)/2$	12.5185	12.5185	12.5185	12.5185	12.5185
$(B_e^{emp})_{eff}$	6291.552	6145.167	6255.0385	6034.8975	6130.6427
$(B_e^{emp})_{eff} \times 2$	12583.104	12308.334	12510.077	12069.795	12261.2854

^a Experimental rotational constants from Table 3 in the main text.

^b $B_e^{emp} = B_0 + \Delta B$

ASTRONOMICAL SEARCH

A. Column Density Calculations

Column densities (and upper limits) were calculated according to Equation S1 following the convention of Hollis et al. (2004), where N_T is the column density, Q is the rotational partition function at the rotational excitation temperature T_{ex} , ΔT_A^* is the observed intensity, ΔV is the linewidth, η_b is the beam efficiency, T_c is the background continuum temperature, $S\mu^2$ is the intrinsic line strength (with transition dipole moment μ), and E_l and E_u are the lower and upper state energies of the transition under consideration.

$$N_T = \frac{Q \left(\frac{1}{2} \sqrt{\frac{\pi}{\ln 2}} \frac{\Delta T_A^* \Delta V}{\eta_b} \right)}{\frac{8\pi^3}{3h} \left(T_{ex} - \frac{T_c}{\eta_b} \right) S\mu^2 (e^{-E_l/kT_{ex}} - e^{-E_u/kT_{ex}})} \quad (\text{S1})$$

From inspection of Equation S1, ΔT_A^* and $\left(T_{ex} - \frac{T_c}{\eta_b} \right)$ must have the same sign for the column density to be positive. As a consequence, absorption (where ΔT_A^* is negative) can only occur if the rotational excitation temperature T_{ex} is lower than the true (beam-corrected) continuum temperature T_c .

In Sgr B2(N), the continuum is dominated at low frequencies (< 80 GHz) by a strong, non-thermal and frequency-dependent continuum, largely due to free-free emission (Hollis et al. 2007). This continuum drops to $T_c \sim 5$ K by ~ 80 GHz before gradually rising to $T_c \sim 23\text{--}35$ K above ~ 350 GHz (see Fig. S1; Belloche et al. 2013, Neill et al. 2014). Because of the strong continuum in the 1 – 50 GHz range covered by PRIMOS, species with low excitation temperatures are often seen in absorption, rather than emission. Indeed, because the energy levels involved in transitions arising in this frequency region are often inherently low in energy, the majority of the species detected in the PRIMOS survey are have relatively cold excitation temperatures ($T_{ex} < 50$ K; Loomis et al. 2013, Zaleski et al. 2013, Hollis et al. 2008).

The structure of Sgr B2(N) is complex, with a warm, compact ($\sim 3\text{--}5''$) molecular hot core, surrounded by a cooler, extended molecular shell (see Fig. S2). The angular extent of this colder shell is not well constrained, although the emission of many molecules in it is well-modeled by a source size of at least $200''$ (Belloche et al. 2013). For molecules seen in absorption, the source size is well-constrained to the angular extent of the background

continuum they are absorbing against, which is $20''$. Because the size of the GBT beam varies significantly over the span of the observations, from $75''$ at 10 GHz to $15''$ at 50 GHz, and the beam is centered on the hot core ([J2000] $\alpha=17^h47^m19^s.8$ $\delta=-28^\circ22'17''$), rather than on the continuum, corrections for beam-dilution must be handled with care. At each frequency, we explicitly calculate the angular scale of either the extended shell or hot core contained within the GBT beam, and use that extent to calculate an appropriate beam-dilution correction factor, B , using Equation S2, where θ_s is the source size and θ_b is the beam size.

$$B = \frac{\theta_s^2}{\theta_s^2 + \theta_b^2} \quad (\text{S2})$$

The telescope beam efficiency (η_b) was calculated explicitly at each frequency across the PRIMOS band using Equation S3 (Hollis et al. 2007).

$$\eta_b = -15.52 \times 10^{-5} \nu^2 - 22.59 \times 10^{-4} \nu + 0.98 \quad (\text{S3})$$

Partition functions for each species were determined by direct summation of energy levels. We note that these partition functions are purely rotational, and no attempt was made to include contributions from vibrational states, as only negligible contribution from such states is expected under typical excitation conditions probed by PRIMOS. Linewidths used to determine upper limits were set uniformly to 10 km/s, a typical value within the source (Belloche et al. 2013).

B. Background Continuum

Figure S1 shows a representation of the background continuum observed toward Sgr B2(N) at various frequencies. The Hollis et al. (2007) measurements have been corrected for beam-dilution effects from the portion of the total $20''$ emitting region contained within the GBT beam at each frequency. The exact corrections, if any, to the values from Belloche et al. (2013) and Neill et al. (2014) are not explicitly clear from the reference literature. The blue and gold traces demonstrate where a molecule with $T_{ex} = 25$ K would display absorption or emission, relative to the background.

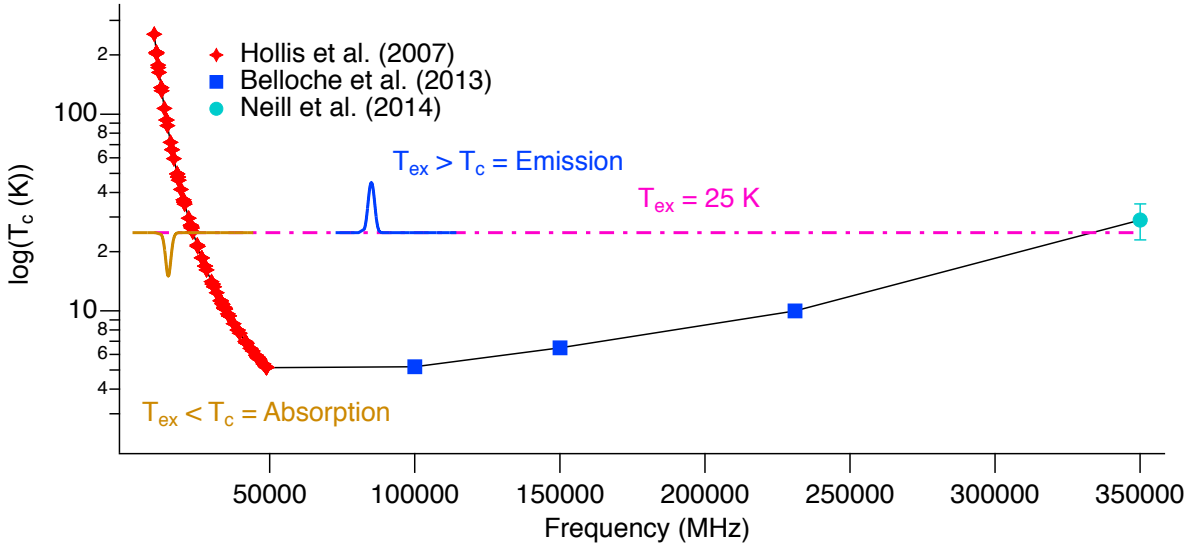


FIG. S1. Measurements of the continuum temperature (T_c) in Sgr B2(N) at various frequencies from Hollis et al. (2007), Belloche et al. (2013), and Neill et al. (2014).

C. Sgr B2(N) Structure

Figure S2 gives a qualitative overview of HSCN in Sgr B2(N). The dotted area represents the cold, extended gas observed both here, and in Halfen et al. (2009). The shaded blue area represents the $\sim 20''$ region which displays continuum emission above the cosmic microwave background (CMB). HSCN beyond this area is observed in emission against the CMB, and an example spectrum at $T_{ex} = 19$ K, as derived by Halfen et al. (2009) (black trace) shows that this emission will peak around ~ 100 GHz, as they observe. The emission falls off rapidly toward lower frequency, and will not significantly contribute to any observed signal in those frequency ranges.

The blue trace shows the effect of a strong background continuum on the observed signal from HSCN. The strongest signal is observed at the lowest frequencies. This is not because the lines themselves are stronger, but rather the background continuum at those frequencies is the greatest, making the measured line-to-continuum ratio (analogous to a percentage absorption) the largest. This intensity falls off as the continuum decreases at higher frequencies (see Figure S1).

It is clear, then, that an observation that encompasses both regions, such as the example $60''$ beam shown in red (a beam size in the range of both the GBT and ARO observations)

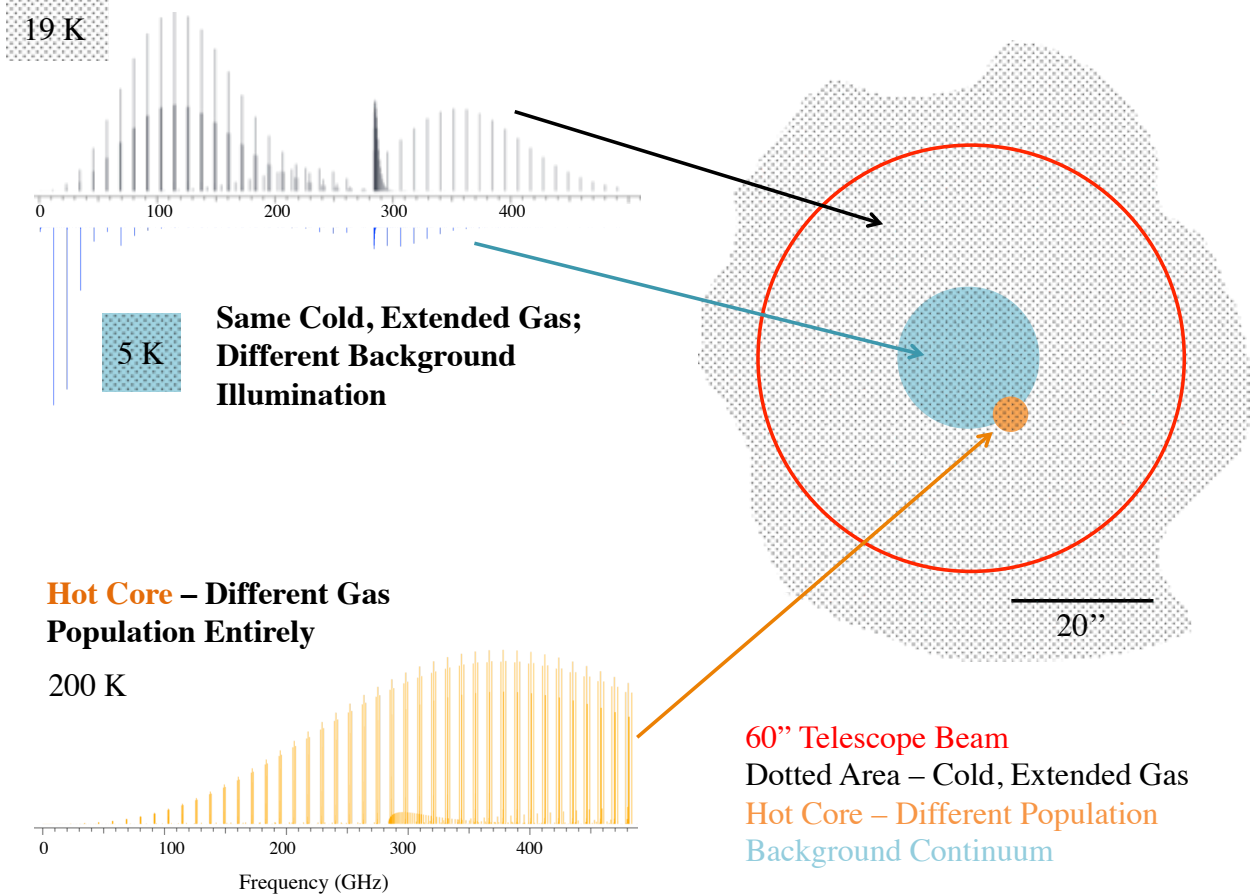


FIG. S2. Qualitative schematic of HSCN in Sgr B2(N).

will see contributions from both types of signal. In the PRIMOS case, the observed signal will generally appear more like the 5 K case, as the PRIMOS observations stop at 50 GHz, below which the absorption signals are dominant. In the case of Halfen et al. (2009), where the observations begin at \sim 69 GHz, the absorption is no longer detectable, and the signal is purely emissive. Thus, when taken individually, low-frequency and high-frequency observations can easily arrive at two different excitation temperatures to describe the absorptive and emissive behavior they see. Nevertheless, these observations are probing the same molecular population.

This is distinct from observations of molecules which reside in the hot core. A simulation of HSCN at 200 K, an excitation temperature typical in the hot core, is provided for illustration only; there has been no reported detection of HSCN under these conditions. If a molecule is present in both the hot core and the colder, extended shell, a two-component model must be used to fit the observed emission at frequencies much above 100 GHz. This

is because both populations will contribute significantly to the observed signal. At low frequencies, only the most abundant, strongest hot core molecules will be visible, as the peak of the emission is far from these regions, and the strong continuum significantly decreases emission signal, even from hot core molecules.